

Low-Cost Computational Modeling of Aeroacoustic Interactions Between Adjacent **Propellers**

de Prenter, Frits; Casalino, D.; Zarri, A.

DOI

10.2514/6.2024-3069

Publication date

Document Version

Final published version

Published in 30th AIAA/CEAS Aeroacoustics Conference (2024)

Citation (APA)

de Prenter, F., Casalino, D., & Zarri, A. (2024). Low-Cost Computational Modeling of Aeroacoustic Interactions Between Adjacent Propellers. In *30th AIAA/CEAS Aeroacoustics Conference (2024)* Article AIAA 2024-3069 (30th AIAA/CEAS Aeroacoustics Conference, 2024). https://doi.org/10.2514/6.2024-3069

Important note

To cite this publication, please use the final published version (if applicable). Please check the document version above.

Copyright

Other than for strictly personal use, it is not permitted to download, forward or distribute the text or part of it, without the consent of the author(s) and/or copyright holder(s), unless the work is under an open content license such as Creative Commons.

Please contact us and provide details if you believe this document breaches copyrights. We will remove access to the work immediately and investigate your claim.



Low-Cost Computational Modeling of Aeroacoustic Interactions between Adjacent Propellers

Frits de Prenter *

Delft University of Technology, Delft, The Netherlands

Alessandro Zarri †

von Karman Institute for Fluid Dynamics, Rhode-St-Genèse, Belgium

Damiano Casalino [‡]
Delft University of Technology, Delft, The Netherlands

Distributed Electric Propulsion systems are an emerging technology. Aerodynamic interactions between propellers in close proximity can, however, cause periodic variations in the blade loading. Together with acoustic interference, these installation effects can form a dominant noise source in such systems. In this contribution, we investigate a low-cost computational modeling approach to predict the unsteady loading of the propeller blades, and thereby the interaction noise of an array of side-by-side propellers. To inform this low-cost model, a numerical campaign of scale-resolving Lattice Boltzmann/Very Large Eddy Simulations (LBM/VLES) has been performed on the Dutch National Supercomputer Snellius. The goal of this model development is to gain a better understanding of the blade-to-blade interaction mechanisms and to determine to which extent the model can be applied for purposes like preliminary design, uncertainty quantification, or control, for which the computational cost of high-fidelity simulations is prohibitive. As a practical example, the optimal relative phase angle in an array of propellers is determined and validated.

I. Introduction

One of the main future challenges in aerospace engineering is the development of aircraft with low emissions of pollutants, greenhouse gasses, and noise [1]. Electrical propulsion systems enable vast advantages with respect to traditional propulsion systems based on fossil fuels in all three of these aspects. Besides the advantages regarding pollutants and greenhouse gases through the use of electrical motors, Distributed Electrical Propulsion (DEP) systems have the potential to improve the efficiency of the propulsion system while reducing the noise production [2]. Such systems consist of an array of propellers distributed along the wingspan, such as the EcoPulse, Vahana, or, X-57 Maxwell [3–5].

Propellers in close proximity are affected by complex interaction effects. In particular, oscillations in the aerodynamic blade loading can be observed [6, 7], which is the result of a tip-to-tip interaction by which a non-uniform inflow generates periodic loads [8]. These oscillations in the blade loading can form a mechanism that dominantly affects the noise production and directivity [9]. Besides this unsteady loading affecting the noise production of a single propeller, constructive and destructive interference effects between the different propellers must be considered in DEP systems [10, 11]. These installation effects must be well understood to enable new aircraft designs with reduced acoustic emissions.

In this contribution, we develop a low-cost approach to compute the interaction noise of adjacent propellers with two main purposes. First, we aim to improve our understanding of the different mechanisms and loading contributions that affect the propeller-to-propeller interaction noise, and what these are influenced by. Second, we strive to determine if the modeling technique is capable of accurately capturing the interaction noise and therefore suitable for purposes like design optimization, for which high-fidelity simulations can be prohibitively expensive. Fig. 1 presents the three-propeller setup employed in this study. In the current study, we only consider a single parameter: the relative phase angle (or the

^{*}Department of Flow Physics and Technology, f.deprenter@tudelft.nl.

[†]Aeronautics and Aerospace Department, alessandro.zarri@vki.ac.be.

[‡]Department of Flow Physics and Technology, d.casalino@tudelft.nl.

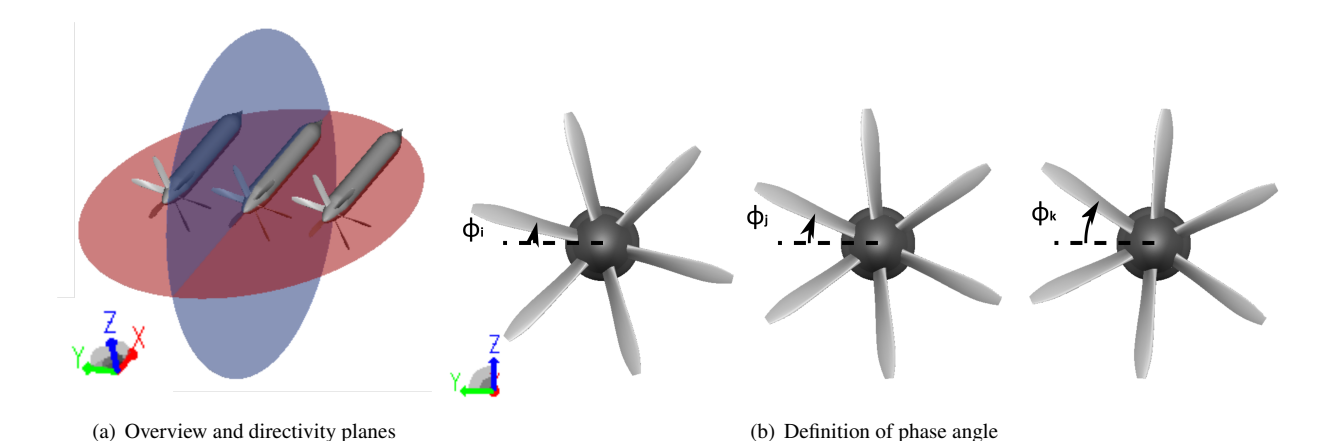


Fig. 1 Overview of the considered three-propeller setup. (a) provides an overview of the setup, the coordinate system, and indicates the planes in which directivity is calculated in later sections. The front view in (b) defines the phase angle, which can vary between the propellers and is the variable parameter considered in this study.

phase-angle difference) between adjacent propellers as defined in Fig. 1(b). This phase angle has a large influence on the noise production [9], and a low-cost technique can be applied to minimize the noise production in situations where the phase difference can be controlled, and can provide an uncertainty quantification for situations where it cannot be controlled.

While this contribution focuses on the installation effect of adjacent propellers on noise production, it should be mentioned that also the aerodynamic performance of DEP systems is a topic of research. Aerodynamically, DEP systems can offer advantages by increasing the low-speed performance [12] and by enabling a spanwise augmentation of the lift [13]. At the same time, however, other studies have shown that, depending on configuration, the close proximity of the propellers can also result in a loss of generated thrust up to 8%, with the highest percentages appearing in hover conditions [14, 15]. For the specific setup employed to generate the data in this contribution, the thrust was reduced by 1.5% with respect to an isolated propeller [16]. In this study, the effect on the thrust is not considered.

This contribution is organized as follows. Section II presents the considered setup and provides a short overview of the setup of the high-fidelity model. Section III describes the low-cost approach to predict the unsteady aerodynamic loading and tonal interaction noise produced by adjacent propellers and provides a validation of the technique. Section IV shows an example application in which the noise of a propeller setup is minimized. Section V provides some concluding remarks.

II. High-fidelity model

The high-fidelity numerical setup of the three-propeller setup defined in Fig. 1 has previously been employed in our past contribution [9]. For this reason, we confine this section to a summary of the main features and refer interested readers to the aforementioned publication. Different from the previous contribution is the simulation duration. This has been extended and here involves 10 propeller rotations in a coarse simulation with only the Variable Resolution (VR) mesh region VR1 to VR8 activated, followed by 12 rotations in a fine simulation with all VR levels active. Furthermore, we have run symmetric cases with both side propellers at the same initial phase angle $\phi = 0^{\circ}$ and the middle propeller at $\phi \in \{0^{\circ}, 2^{\circ}, 5^{\circ}, 10^{\circ}, 20^{\circ}, 30^{\circ}, 40^{\circ}, 50^{\circ}, 55^{\circ}, 58^{\circ}\}$ to inform the low-cost model. Note that with 6 blades a phase difference of 60° is equal to exactly shifting one blade and is equivalent to a phase difference of 0° . Additionally, we have run non-symmetric validation cases with the [left, middle, and right] propeller initially at $[0^{\circ}, 10^{\circ}, 20^{\circ}]$ and at $[29^{\circ}, 0^{\circ}, 36.5^{\circ}]$.

The setup contains propellers of the TUD-XPROP-S type, with a radius of 101.6 mm, a root chord of 16.287 mm, and 6 blades. The nacelles are taken as in the experiments in [16] and have a length of 3.7 times the radius. The tip-to-tip clearance is 4.064 mm (4% of the radius), and the propellers are co-rotating in the negative x-direction. The free-stream velocity of the inflow is set to $V_{\infty} = 30$ m/s, with a static pressure and temperature of $p_{\infty} = 101330$ Pa and $T_{\infty} = 288.15$ K. The advance ratio is set to $J = V_{\infty}/nD = 0.8$ resulting in a tip Mach number of M = 0.358 (with n = 184.5 s⁻¹ the shaft frequency).

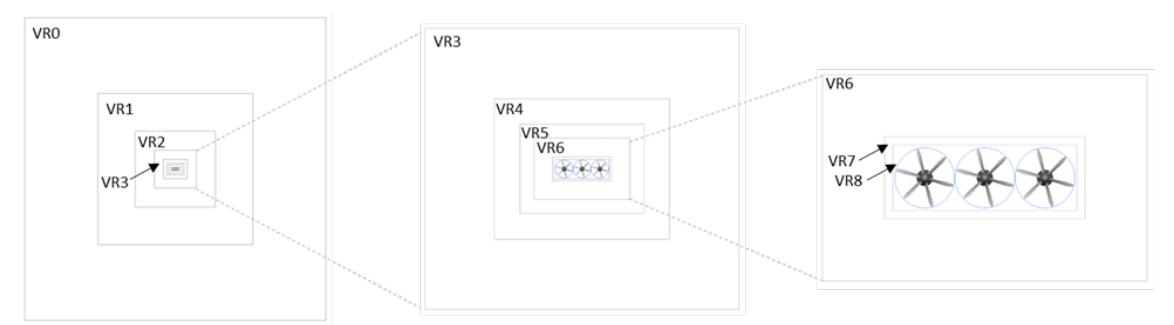


Fig. 2 VR levels in the background (stationary) mesh.

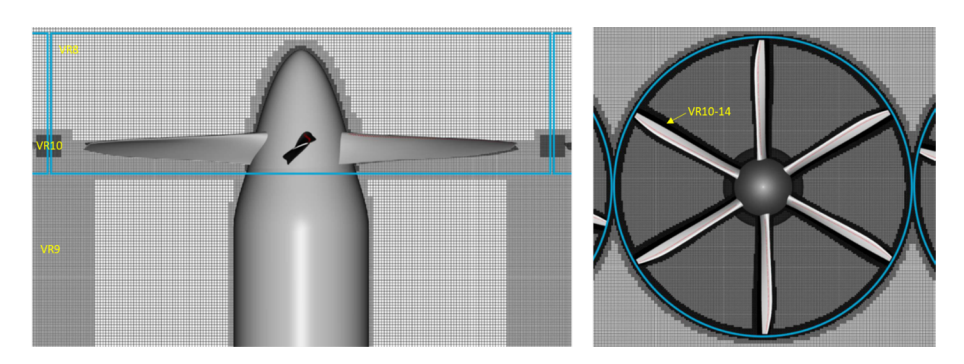


Fig. 3 VR regions in LRF and the hollow cylinder VR9 region in the slipstream to capture the tip vortices.

The high-fidelity simulations are carried out with the high-subsonic solver of the commercial package PowerFLOW, version 6-2022-R3. It employs a Lattice Boltzmann discretization, coupled with a Very Large Eddy Simulation (VLES) turbulence model and an energy equation with a Lax-Wendroff finite difference scheme on the same mesh [17]. The simulation employs 15 Variable Resolution regions (VR), with a voxel size varying from h_0 =0.294 m to h_{14} =17.9 μ m and a total of approximately 22.5 million voxels for the three propeller setup. The stationary (background) mesh contains VR levels 0 to 9, with finer grids towards the propellers (Fig. 2, hollow cylinders of VR9 to capture tip vortices in the slipstream are not shown in this figure but are visible in Fig. 3). A set of three Local Reference Frame (LRF) regions is employed in the vicinity of the propellers containing the finest VR levels (8 to 14), including blade offset layers (Fig. 3). A trip is employed on the suction side at 10% of the leading edge to force the VLES solver to switch from modeling the turbulence with a RANS-type model to resolving it with a LES-type model [18–20]. The computational cost of a single rotation of a single propeller is approximately 3.1k cpu hours, resulting in 112k cpu hours for 12 rotations or the three-propeller setup. The full details of the numerical setup can be found in [9].

III. Low-cost model setup

In this section, we describe and validate the low-cost model informed by the high-fidelity simulations. Section III.A describes how blade loading data is extracted from PowerFLOW and projected to a basis, after which this is converted to noise using a moving-dipole formulation in Section III.B. In Section III.C we demonstrate how the blade loading on a middle propeller in a non-symmetric setup can be approximated using superposition and Section III.D explains the interpolation procedure to obtain the blade loading with a neighboring propeller at any phase difference.

A. Blade loading projection

The blade loading is extracted from the simulations for each blade in 100 annular segments for the three last rotations in time increments equivalent to a rotation of 2° . The results are then averaged over the different blades and phase-locked averaged over the three rotations to obtain the azimuthal thrust and drag distributions. In Fig. 4 and 5 we display the difference of these distributions for the central propeller w.r.t. an isolated propeller, to highlight the unsteady loading. Next, a projection (in L2) of the loading on a set of basis functions is applied to smooth the results in the radial direction

(Fig. 5) and to enable interpolation between results with neighboring propellers at different relative phase angles. The employed basis consists of 10 quadratic radial B-splines with a uniform knot vector and 45 harmonic azimuthal modes. The circumferential strips in the raw CFD results are an artifact of the post-processing script. More specifically, the force on surface elements that intersect with two different annular intervals is not distributed over these, but instead is added in whole to one of the intervals. Because the isolated propeller loading is obtained for a propeller that has a different alignment with the LBM grid than the installed propeller and the unsteady loading is smaller than the steady loading, this causes the observed effect. The projection on the radial spline basis smooths the distribution and resolves this artifact. Note that the tangential lines are not present in Fig. 4 since the installed propeller in that simulation had the same grid alignment as the isolated one.

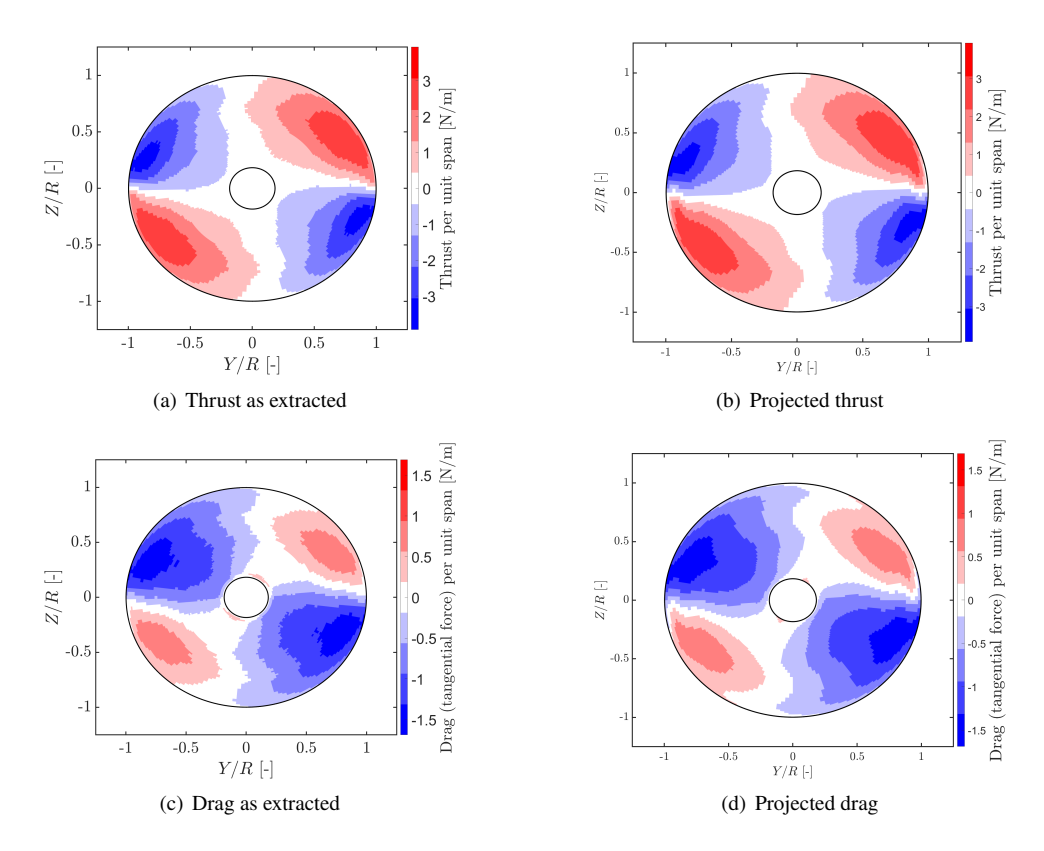


Fig. 4 Differences in thrust and drag (tangential force) distribution of the middle propeller with respect to an isolated propeller for the setup with all propellers at the same phase. Figures (a) and (c): forces as extracted from PowerFLOW. Figures (b) and (d) radial/azimuthal projections.

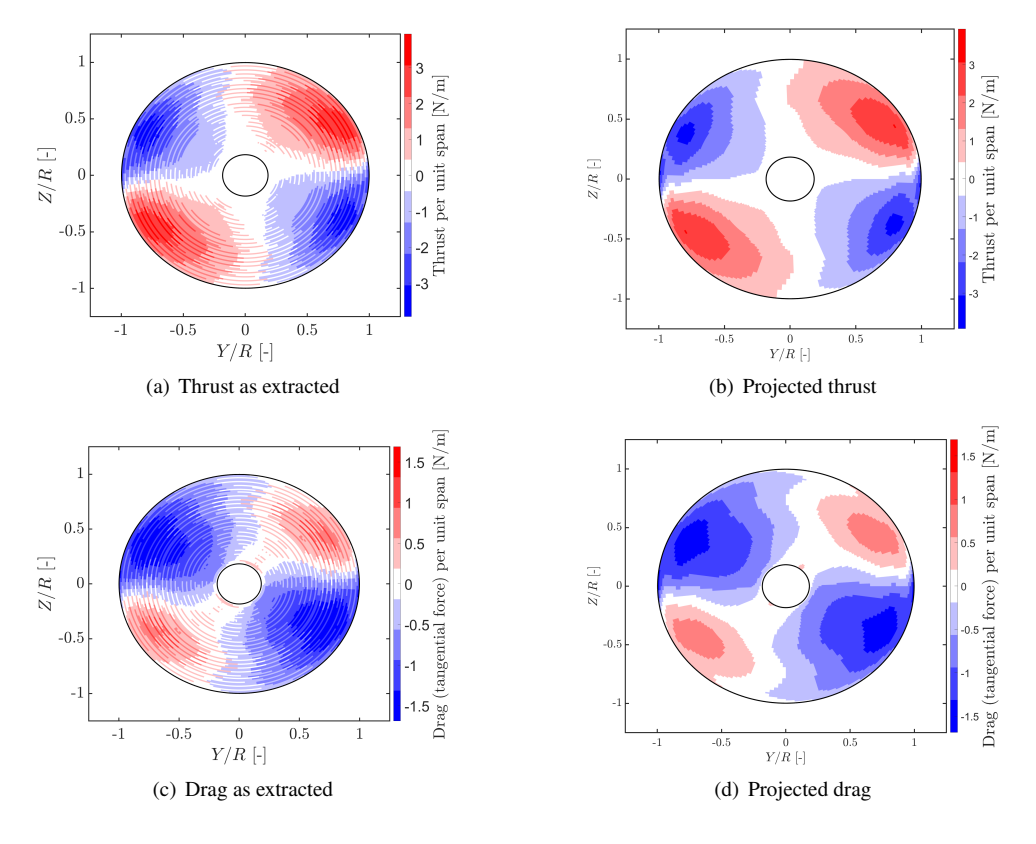


Fig. 5 Differences in thrust and drag (tangential force) distribution of the middle propeller with respect to an isolated propeller for the setup with a phase difference of 30° (fully out-of-phase). Figures (a) and (c) display the phase-locked average directly as extracted from PowerFLOW. Figures (a) and (c): forces as extracted from PowerFLOW. Figures (b) and (d) radial/azimuthal projections.

B. Moving dipoles

We compute tonal noise from the azimuthal force distributions using a rotating dipole model involving 50 dipoles evenly distributed over the radius. This approach is appropriate as the blade segments are acoustically compact because for the considered BPF harmonics the acoustic wavelength is much longer than the chord. This model was introduced in [21] and the formulation used here is adopted from [22]

$$\hat{P}(mB\Omega) = \frac{-iB^2 \Omega e^{-imB\Omega R_{\text{mic}}/c}}{4\pi R_{\text{mic}}c} e^{-imB\phi} \sum_{p=-\infty}^{p=\infty} e^{-i(mB-p)(\zeta-\pi/2)} \left(J_{mB-p} \left(mBM \sin(\theta) \right) \left(m \cos(\theta) \hat{F}_t(p\Omega) - \frac{mB-p}{BM} \hat{F}_d(p\Omega) \right) \right)$$

$$- J'_{mB-p} \left(mBM \sin(\theta) \right) im \sin(\theta) \hat{F}_r(p\Omega) \right)$$

$$(1)$$

with $\hat{P}(\cdot)$, $\hat{F}_t(\cdot)$, $\hat{F}_d(\cdot)$, and $\hat{F}_r(\cdot)$ the Fourier transforms of the acoustic pressure at the microphone position, the thrust, the tangential force (drag), and the radial force of a dipole. m denotes the BPF harmonic, B the number of blades, R_{mic} the microphone distance from the center of the propeller, c the speed of sound, M the mach number of the blade segment, and $J_i(\cdot)$ the ith Bessel function of the first kind. The angles ζ and θ define the direction of the microphone and are indicated in Fig. 6 and ϕ indicates the initial phase angle of the propeller as defined in Fig. 1. Thickness noise can be neglected and is not included in the model [23]. Forces in the radial direction are generally not considered in moving dipole models, but while not dominant in the noise production, unsteady radial forces were observed to play a role in the interaction noise, maximally contributing up to approximately 1 dB. By including these a near-perfect fit with the FWH postprocessing tool implemented in PowerFLOW is observed as visible in Fig. 7, which presents the sound pressure level (SPL) of the 1st and 2nd BPF harmonic in dB. The microphones are placed in a circular array at a radial distance of 20.32 m (100 times the propeller diameter) in a plane spanned by the horizontal coordinates (red plane in Fig. 1(a)) with 0° pointing upstream of the propellers. The pattern of destructive interferences in Fig. 7(b) and Fig. 7(d) is explained by the wavelength of the second BPF harmonic (0.149 m) and the heart-to-heart distance between the propellers (0.207 m).

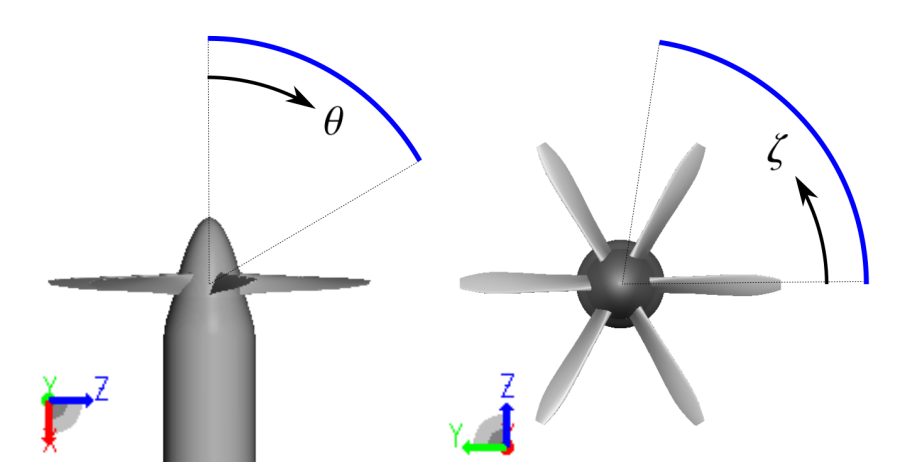


Fig. 6 Definition of microphone angles θ and ζ .

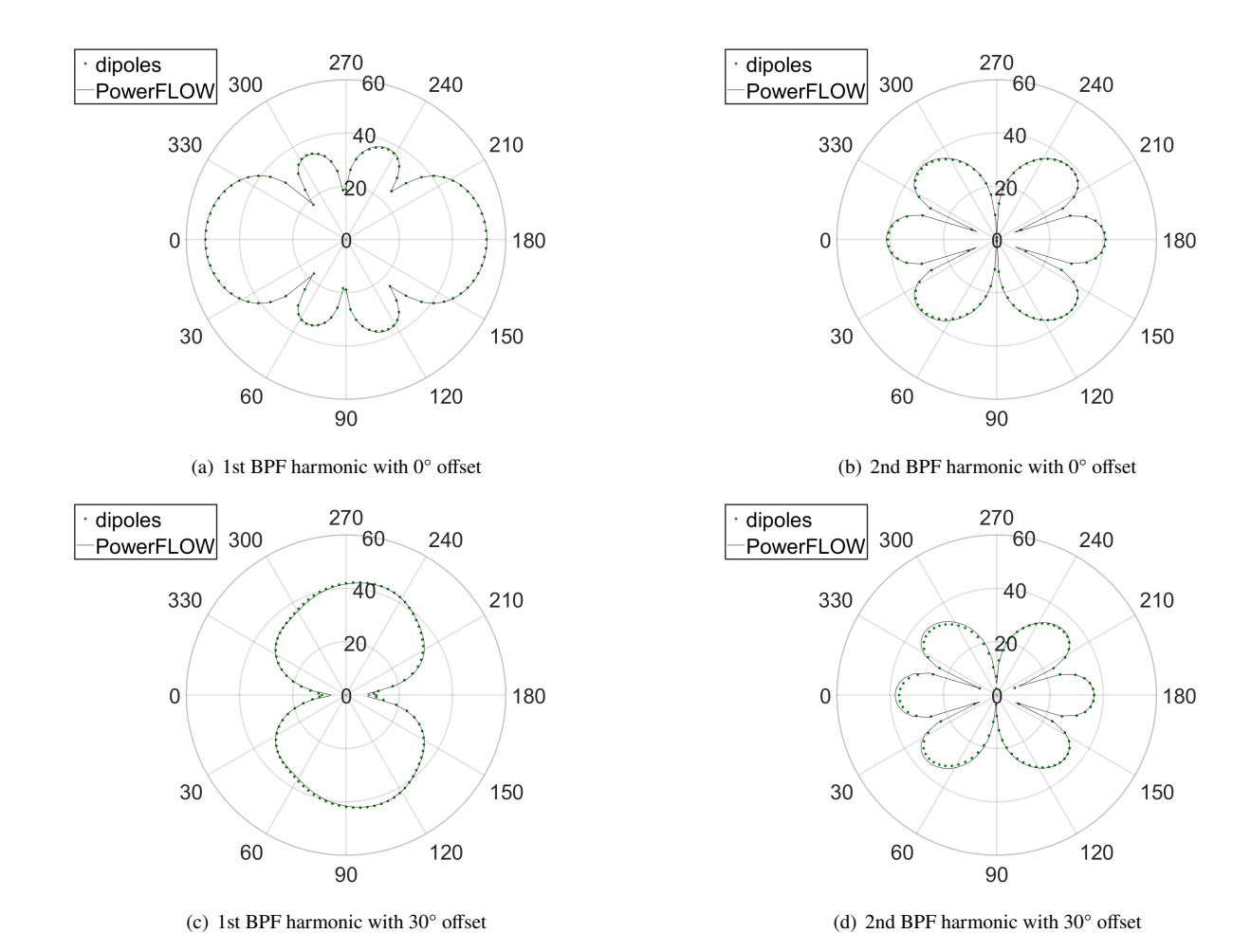


Fig. 7 Comparison between the dipole formulation and the FWH formulation implemented in PowerFLOW.

C. Superposition of unsteady blade loading

To enable the prediction of blade loading on the middle propeller for non-symmetric cases where the phase angle of the left neighboring propeller is not equal to the phase angle of the right neighboring propeller (without having to feed the model with simulations of all possible combinations), we superpose the separate contribution of the left and right neighboring propeller to the unsteady loading of the middle propeller. The superposition of the separate contributions of the neighboring propellers is validated against a simulation with the left propeller at a phase gain of 10° w.r.t. the middle propeller and the right propeller at a phase lag of 10° w.r.t. the middle propeller. Fig. 8 shows the blade loading and Fig 9 shows the directivity of the noise produced by the middle propeller in dB for the same microphone array as in Fig. 7.

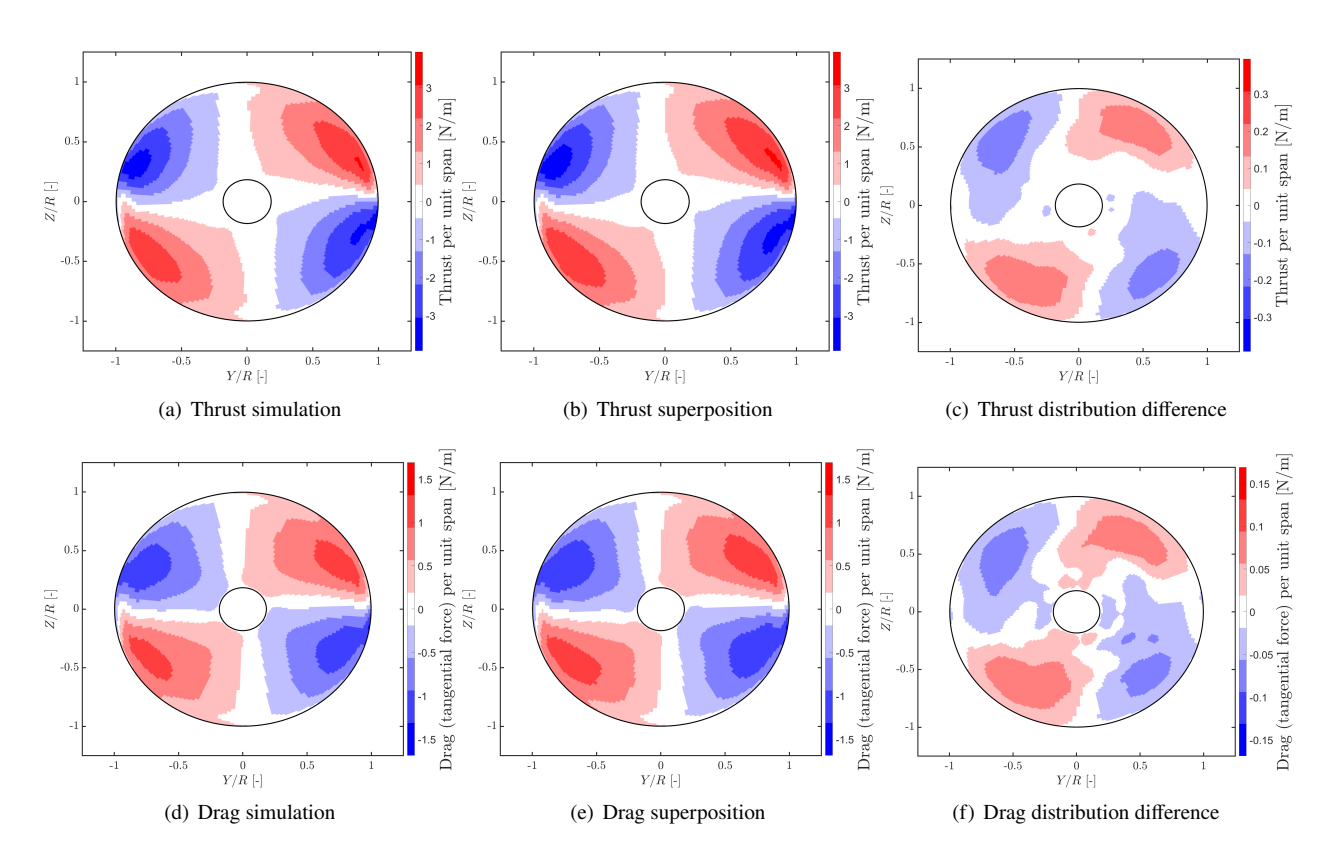


Fig. 8 Validation of the superpositioning of unsteady loading from neighboring propellers on both sides. Note that (c) and (f) have different scales.

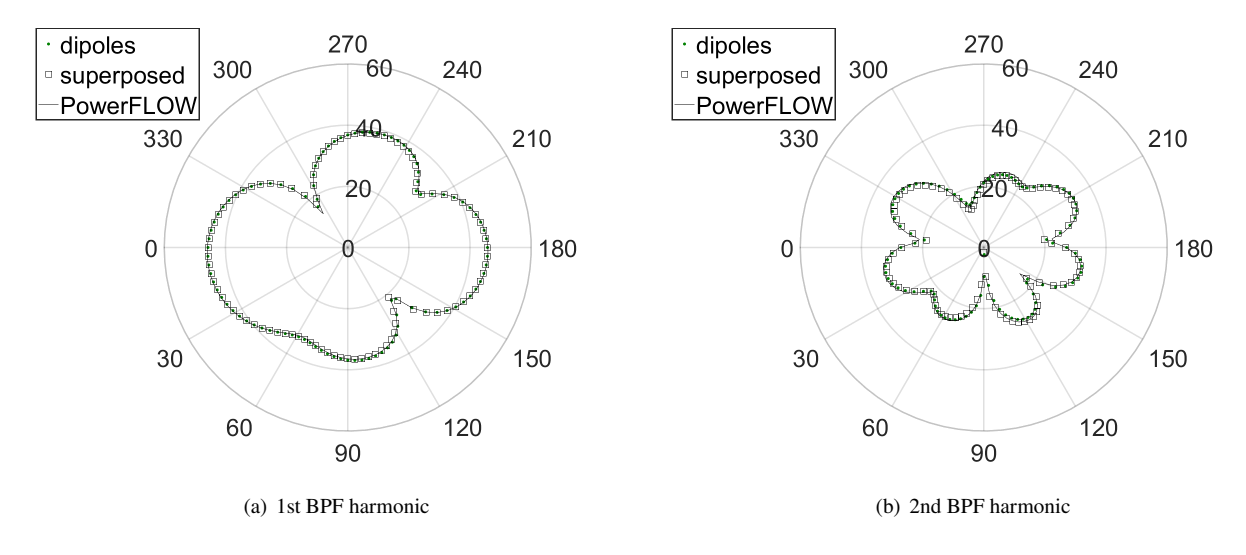


Fig. 9 Validation of the low-cost noise prediction model based on the unsteady loading superposition on both sides of the central propeller. Legend entries *dipoles* and *superposed* employ the dipole formulation based on blade loading obtained through, respectively, the validation simulation and superposition. Legend entry *PowerFLOW* employs the FWH formulation implemented in PowerFLOW.

D. Interpolation between simulated phase differences

To compute the blade loading caused by a neighboring propeller also at phase differences that were not simulated, we interpolate the blade-loading coefficients that were obtained in the projection of the loading on the B-spline (radial coordinate) and harmonic (azimuthal coordinate) basis. The harmonic blade loading distribution can be defined by different bases, from which we choose the following with for each azimuthal mode a magnitude and a shift as coefficients

$$f(r,\theta) = \sum_{1 < n_r < N_r} \sum_{0 < n_a < Na} \alpha_{n_r,n_a} B_{n_r}(r) \cos(n_a \theta + \gamma_{n_r,n_a}), \tag{2}$$

with n_r the number of the quadratic radial B-spline, $B_{n_r}(\cdot)$ the B-spline function, $N_r = 10$, n_a the number of the azimuthal harmonic, $N_a = 45$, and the blade-loading coefficients denoted by $0 \le \alpha_{n_r,n_a}$ the real positive magnitude and γ_{n_r,n_a} the azimuthal shift. We prefer using this basis over a basis consisting of e.g., a separate sine and cosine contribution, since the presented basis allows a more natural interpolation of the coefficients. For example, a mode that has the same magnitude α_{n_r,n_a} but a different shift γ_{n_r,n_a} with neighbors at different relative phase angles, will maintain its magnitude when interpolating coefficients in this basis, while the magnitude would decrease with a basis consisting of separate sine and cosine contributions.

The coefficients are interpolated between simulated phase differences using another quadratic B-spline basis with knot vector (2°, 10°, 30°, 50°, 58°) that is periodic at the outer boundaries of 0° and 60° (note that the propellers have 6 identical blades, such that neighboring propellers at a relative phase difference of 60° and 0° are the same). The knot vector has a higher resolution around the (periodic) boundary as larger variations in the blade loading are observed here, which also motivated to augment the dataset that originally included the phase differences of {0°, 10°, 20°, 30°, 40°, 50°} between the middle and the side propellers with additional simulations at $\{2^{\circ}, 5^{\circ}, 55^{\circ}, 58^{\circ}\}$. Figure 10 displays the interpolation of the magnitude and shift of the coefficient corresponding to the 1st BPF harmonic at the 10th (outer) radial B-spline of the drag. As the azimuthal shift γ_{n_r,n_a} is periodic (the blade loading does not change when 360° is added or subtracted), it can be interpolated in two directions as illustrated in Fig. 11. In case subsequent shift coefficients obtained from the simulated phase differences are more than 180° apart, therefore 360° is added or subtracted to one of the simulated shifts such that we interpolate in the closest direction, as displayed in Fig. 12(a) which corresponds to the 2nd radial B-spline and the 9th shaft harmonic of the drag (the open circles mark the originally obtained values). For some modes this results in a $n \cdot 360^{\circ}$ mismatch between the shift at a phase difference of 0° and 60° , as displayed in Fig. 12(b) for the 1st (inner) radial B-spline and the 1st BPF harmonic of the thrust. It should be mentioned that for some coefficients a very bad relative fit is obtained. This is, however, only the case for modes that have a marginal contribution to the loading, such that we are basically fitting numerical noise, and these modes do not significantly affect the blade loading or noise production. Since the loading of the left and right propellers is (rotational) symmetric in the symmetric setups that were simulated to inform the model, the simulation data from the side propellers is averaged. The simulation data from the middle propeller is not employed in the model and is only used for validation purposes.

The interpolation between the phase differences of a neighboring propeller is validated with a simulation of a right propeller that has an initial phase angle of 36.5° while the middle propeller has an initial phase angle of 0°. Fig. 13 presents the blade loading and Fig. 14 presents the noise directivity in dB for the same microphone array as in Fig. 7.

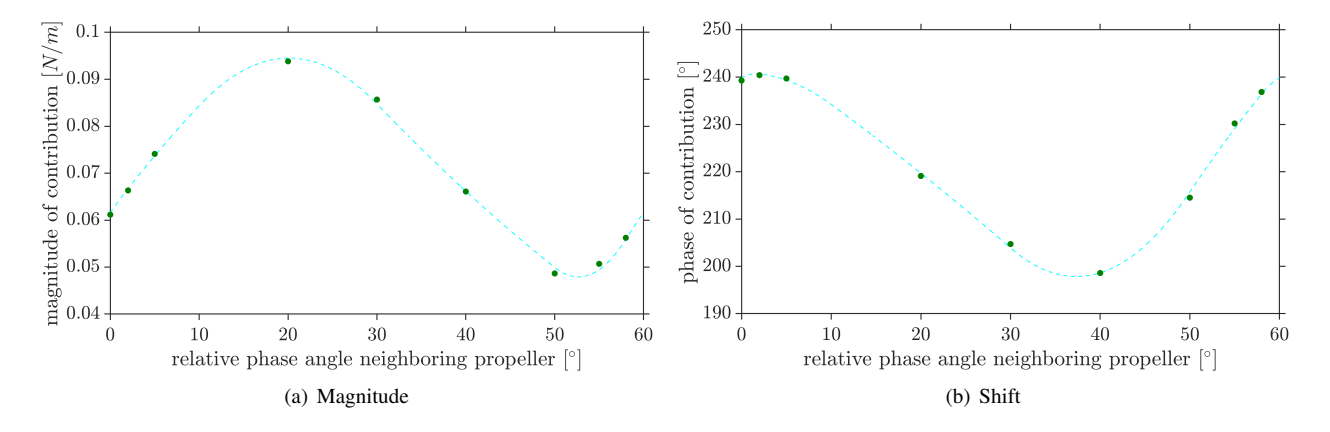


Fig. 10 Interpolation of the magnitude and shift coefficients corresponding to the 1st BPF harmonic and the 10th radial B-spline function of the drag.

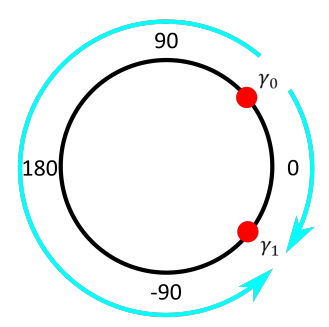


Fig. 11 Example of different interpolation directions from γ_0 to γ_1 .

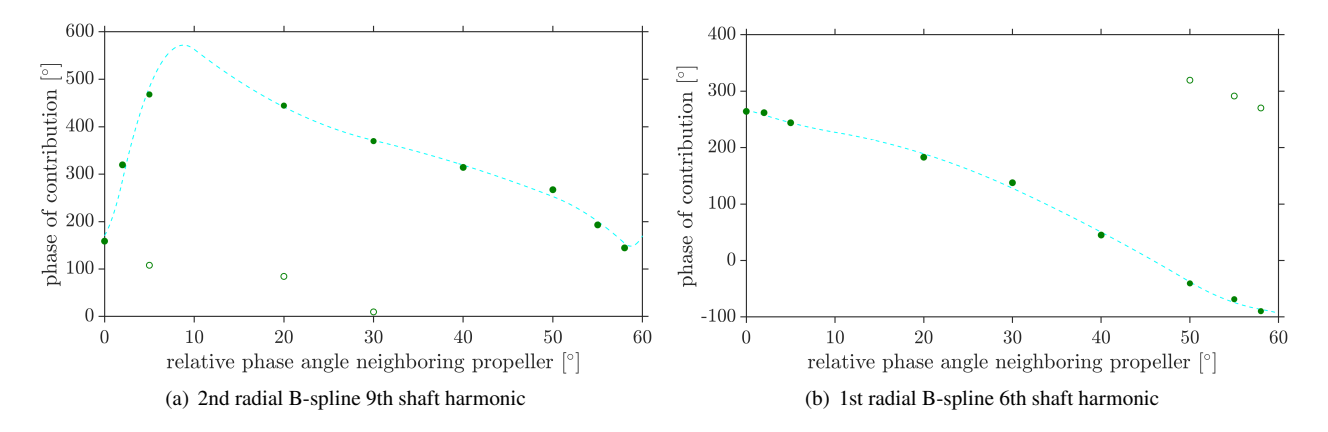


Fig. 12 Interpolation of the shift coefficients with $n \cdot 360^{\circ}$ added to or subtracted from the data points such that interpolation takes place in the closest direction.

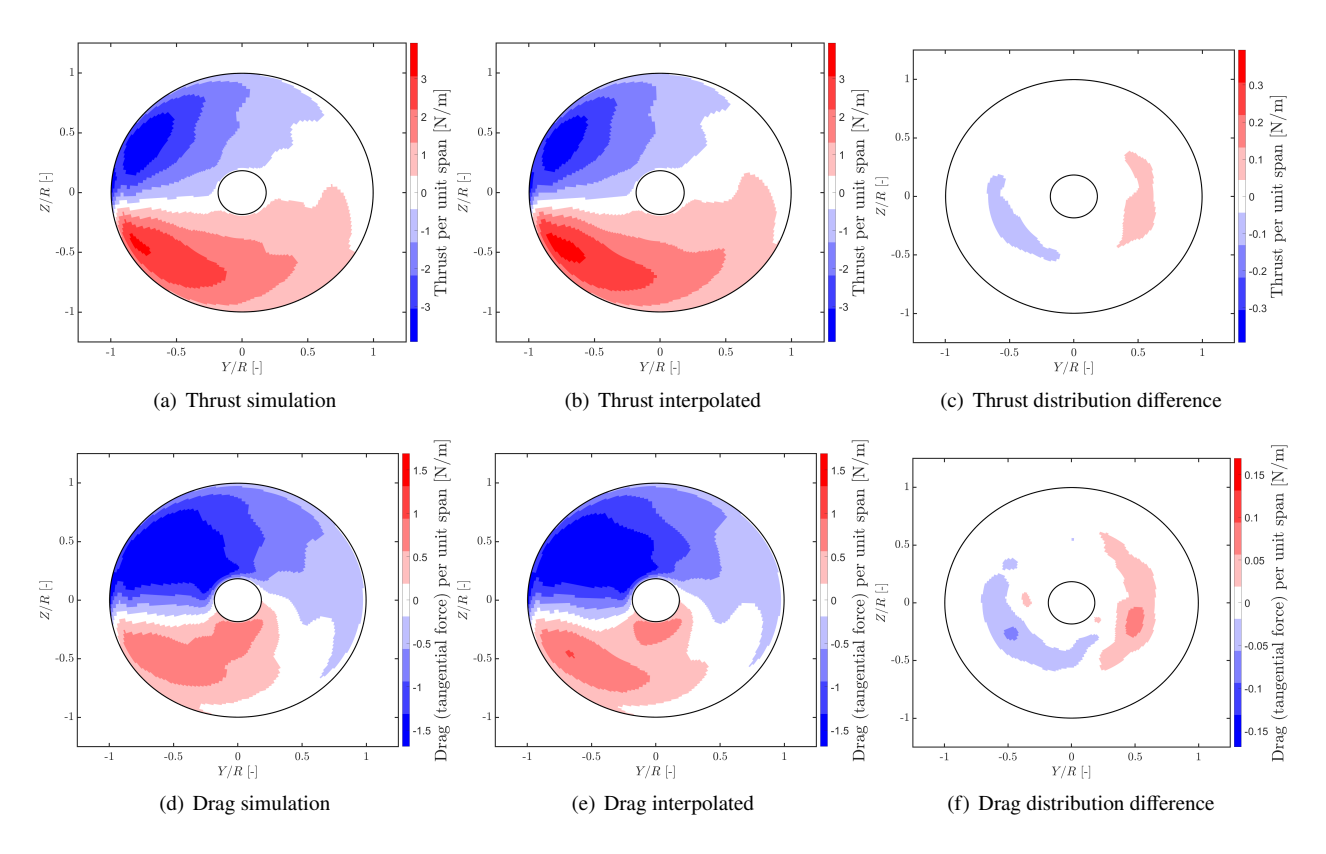


Fig. 13 Validation of the unsteady loading interpolation for a right propeller with a phase difference of 36.5°. Note that (c) and (f) have different scales.

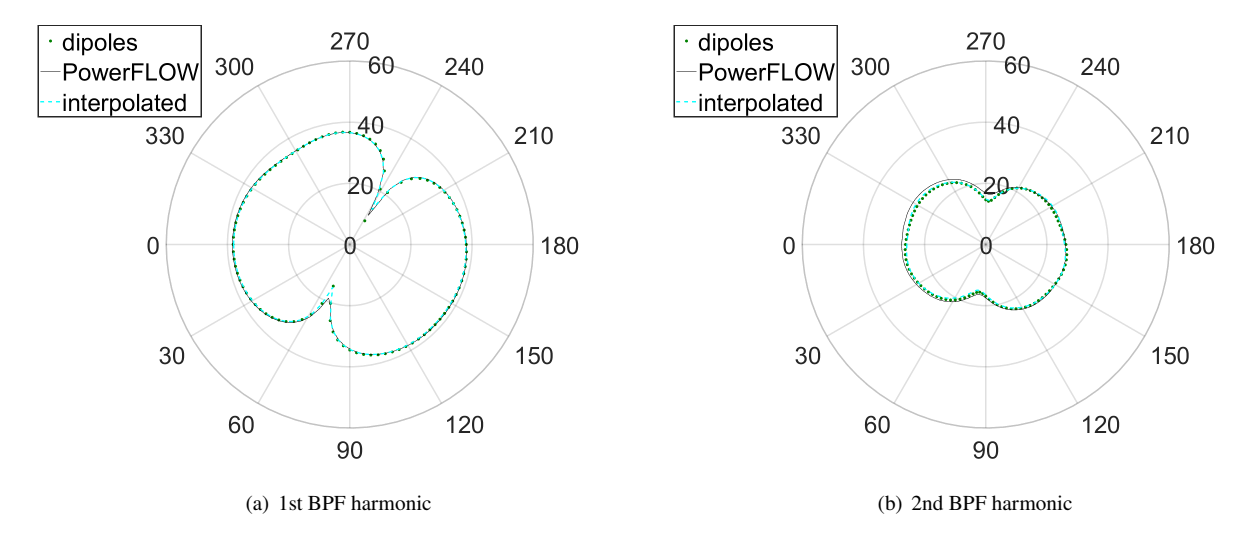


Fig. 14 Validation of the noise production of the right propeller with unsteady loading coefficients interpolated between the simulated phase differences. Legend entries *dipoles* and *interpolated* employ the dipole formulation based on blade loading obtained through, respectively, the validation simulation and interpolation. Legend entry *PowerFLOW* employs the FWH formulation implemented in PowerFLOW.

IV. Application example: noise in lower hemisphere

To demonstrate an application of the data-driven low-cost model, we compute the tonal far-field sound power level (PWL) in the lower hemisphere (Z<0) for all possible combinations of initial phase angles of the left and right propeller. The PWL computation is based on the first 5 BPF harmonics (the first 2 dominate the PWL) using 1024 (virtual) microphones. The computation of the blade loading of a single propeller and evaluation of the noise at all microphones takes approximately 9 seconds on a single cpu. The results are presented in Fig. 15. The maximum PWL of 80.9 dB is obtained with both the left and right propeller at 3.5° and is close to the PWL with all propellers exactly in phase which yields 80.8 dB. The minimum PWL is obtained with the left propeller at an initial phase angle of 29° and the right propeller at an initial angle of 36.5° and yields 76.7 dB. Note the asymmetry in the results, which is caused by only evaluating the noise in the lower hemisphere. The minimum noise is close to the noise of a system where the propellers are perfectly out-of-phase with both the left and right propeller at 30°, which yields 77.0 dB.

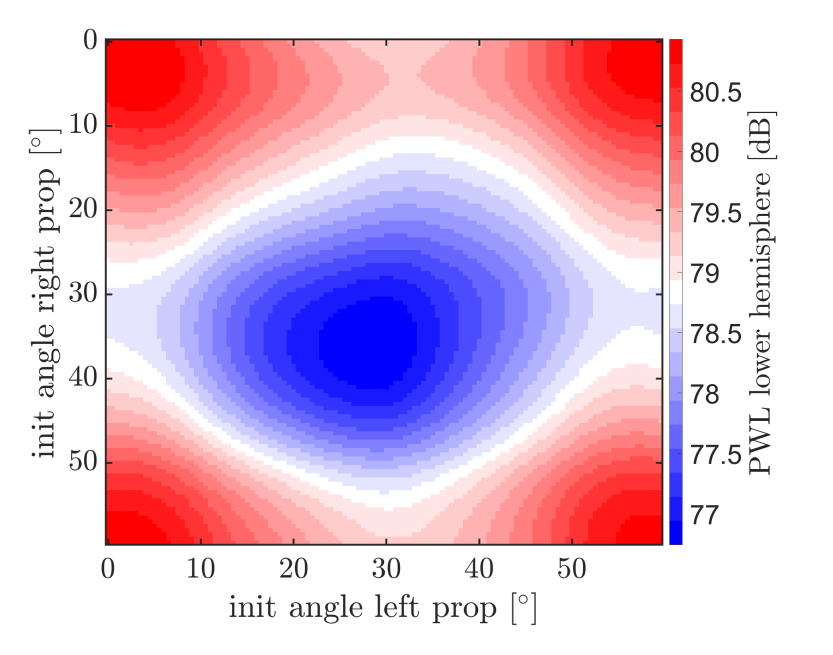


Fig. 15 PWL in lower hemisphere vs. initial phase angle of left and right propeller.

To provide a deeper evaluation of the extreme cases, we have plotted the distribution of the tonal sound pressure level (SPL) involving the first 5 BPF harmonics over the lower hemisphere in Fig 16. A final validation of the model is done by performing a simulation of the optimal setup and comparing the directivities of the first and second BPF harmonic in dB in the horizontal plane (red plane in Fig. 1(a) as in Figs. 7, 9 and 14) and the vertical plane (blue plane in Fig. 1(a)). The results are presented in Fig 17. The 0° direction in these plots is the upstream direction, such that the flow in the figures is from left to right. A destructive interference of the SPL of the first BPF in the 30° setup can be noticed in the axial direction (at 0° and 180°) in both Figs. 17(a) and 17(c). The only noise contribution in this direction is the unsteady thrust component of the same frequency. This unsteady thrust component at the first BPF is exactly out-of-phase for a pair of interacting propellers at a 30° phase difference.

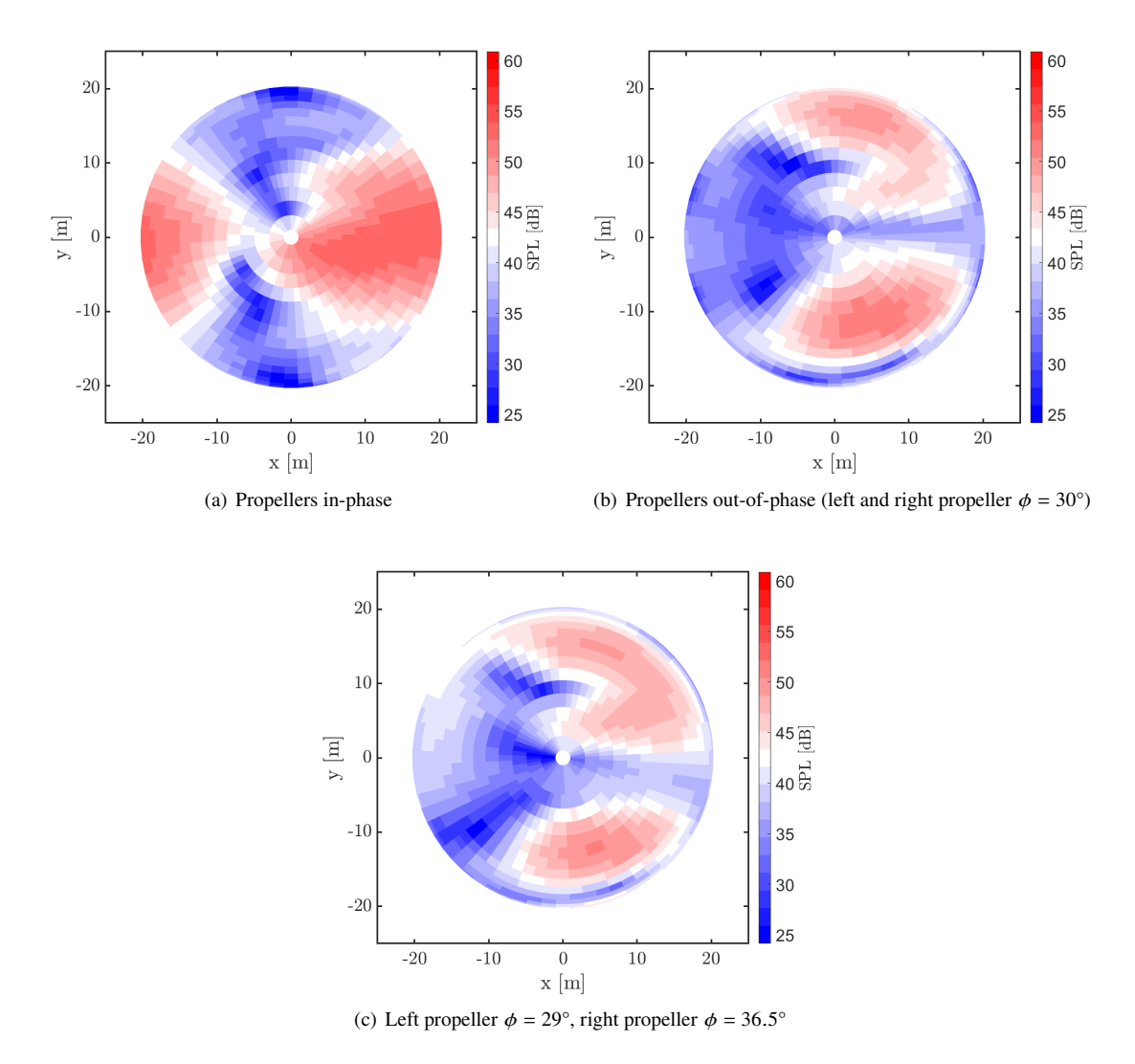


Fig. 16 Tonal SPL distribution on lower hemisphere for various setups. Microphones are at 20.32 m (100 times the propeller diameter). The flow direction is the positive x direction.

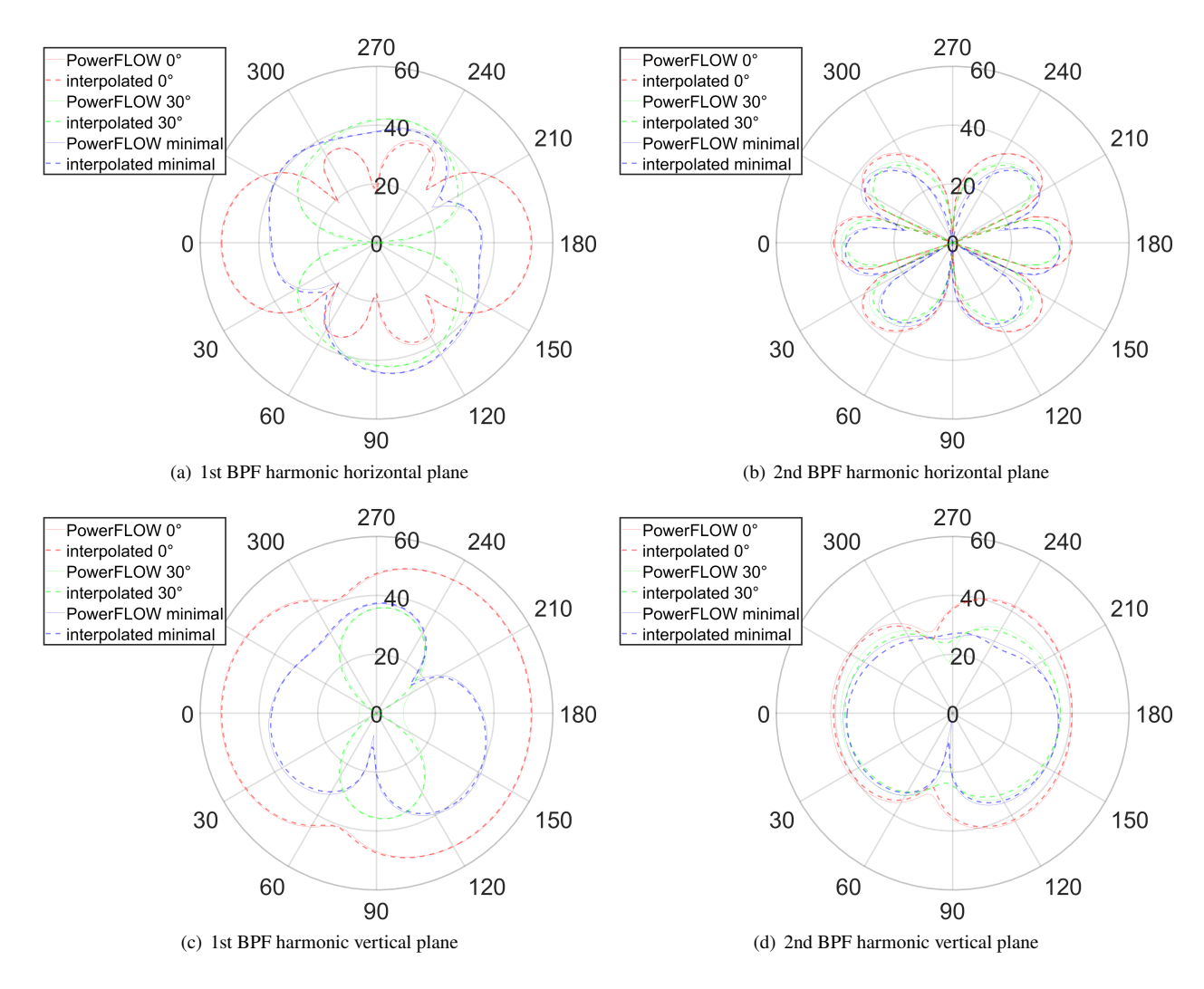


Fig. 17 Validation of the noise directivity of the three-propeller setup of the superposed and interpolated rotating-dipole model vs. the FWH routine implemented in PowerFLOW directly applied to the CFD results for in-phase (0°) , out-of-phase (30°) and minimal noise production (left propeller at 29° and right propeller at 36.5°).

V. Concluding remarks

In this contribution, we have investigated a low-cost computational modeling approach to calculate the interaction noise of an array of adjacent propellers. The model is informed by a set of 10 high-fidelity simulations of propellers interacting with a single neighbor at different relative phase angles. The blade loading from these simulations is projected on a basis to obtain coefficients that can be superposed and interpolated, such that the interaction noise of an array of propellers with any phase difference can be calculated. The overall conclusion is that the model accurately captures the interaction noise of propeller arrays. We presented a validation of the model against high-fidelity simulations and demonstrated how the model can be used to minimize noise production. Besides this, the modeling approach could be applied for various purposes such as (near) real-time noise prediction (for e.g., route planning) or for uncertainty quantification in setups where the relative phase angle cannot be controlled. Additionally, the model can be used to gain a better understanding of the noise-production mechanisms by e.g., assessing the separate contributions of lift, drag, and radial forces on the propeller blades.

Since the overall conclusion is that the modeling approach can accurately compute the noise production, in future steps we intend to expand to model to include more parameters than just the initial phase angle. Given a propeller array, the model could also consider the inflow velocity, angle of attack, and RPM. For the design of a propeller array, this could additionally include parameters like the propeller-to-propeller distance and several parameters involved in the propeller design. When furthermore a wing is considered, also the placement of the propellers with respect to the wing can be added to the degrees of freedom. Incorporating just a fraction of these parameters will result in a prohibitive computational cost if a full-vectorial set of high-fidelity simulations needs to be performed to inform the model. Therefore, we aim to also investigate the application of more elaborate forms of multivariate Design of Experiments to inform the interpolation model, and optionally consider other interpolation techniques such as e.g., machine learning tools. Finally, we intend to investigate if some components of the interaction noise can be well-captured (in quantitative or only in qualitative form) by low-fidelity approaches such as panel or lifting-line techniques, which can then be used to augment design optimization with a Multi-Fidelity Optimization technique like Kriging.

Acknowledgments



This project has received funding from the European Union's Horizon 2020 research and innovation program under grant agreement no 860103 (ENODISE) and the Horizon Europe research and innovation program under grant agreement no. 101138209 (eVTOLUTION).



The computations in this work used the Dutch national e-infrastructure with the support of the SURF Cooperative using grant no. EINF-6653. The research of Frits de Prenter is supported by the NWO Veni scheme grant no. 20153 (STABILIZE).

References

- [1] European Commission Directorate-General for Mobility and Transport and Directorate-General for Research and Innovation, "Flightpath 2050: Europe's vision for aviation," 2011. https://doi.org/10.2777/50266.
- [2] NASA, "Strategic Implementation Plan: 2017 Update," 2017. URL https://www.nasa.gov/wp-content/uploads/2017/04/sip-2017-03-23-17-high.pdf?emrc=46b8c6.
- [3] "EcoPulse," https://www.daher.com/en/ecopulse, Accessed: 19-4-2024.
- [4] "Vahana," https://www.airbus.com/en/innovation/low-carbon-aviation/urban-air-mobility/cityairbus-nextgen/vahana, Accessed: 19-4-2024.
- [5] Litherland, B. L., Borer, N. K., and Zawodny, N. S., "X-57 Maxwell High-Lift Propeller Testing and Model Development," *AIAA AVIATION 2021 FORUM*, 2021. https://doi.org/10.2514/6.2021-3193.
- [6] Lee, H., and Lee, D.-J., "Rotor interactional effects on aerodynamic and noise characteristics of a small multirotor unmanned aerial vehicle," *Physics of Fluids*, Vol. 32, No. 4, 2020. https://doi.org/10.1063/5.0003992.

- [7] Zarri, A., Dell'Erba, E., Munters, W., and Schram, C., "Aeroacoustic installation effects in multi-rotorcraft: Numerical investigations of a small-size drone model," *Aerospace Science and Technology*, Vol. 128, No. 107762, 2022. https://doi.org/10.1016/j.ast.2022.107762.
- [8] Zarri, A., Dell'Erba, E., Munters, W., and Schram, C., "Fuselage scattering effects in a hovering quadcopter drone," 28th AIAA/CEAS Aeroacoustics 2022 Conference, 2022. https://doi.org/10.2514/6.2022-3031.
- [9] Zarri, A., Koutsoukos, A., Avallone, F., de Prenter, F., Ragni, D., and Casalino, D., "Aerodynamic and Acoustic Interaction Effects of Adjacent Propellers in Forward Flight," AIAA AVIATION 2023 Forum, 2023. https://doi.org/10.2514/6.2023-4489.
- [10] Roger, M., "On Combined Propeller Synchronization And Edge Scattering For The Noise Reduction Of Distributed Propulsion Systems," 26th International Congress on Sound and Vibration, 2019.
- [11] Lade, T., Guèrin, S., Zarri, A., and de Prenter, F., "Analysis of Acoustic Interference in Multi-Rotor Propulsion," DAGA 2024, 2024.
- [12] Kummer, J., and Dang, T., "High-Lift Propulsive Airfoil with Integrated Crossflow Fan," *Journal of Aircraft*, Vol. 43, 2006, pp. 1059–1068. https://doi.org/10.2514/1.17610.
- [13] Kim, H. D., Perry, A. T., and Ansell, P. J., "A review of distributed electric propulsion concepts for air vehicle technology," 2018 AIAA/IEEE Electric Aircraft Technologies Symposium (EATS), 2018. https://doi.org/10.2514/6.2018-4998.
- [14] Zhou, W., Ning, Z., Li, H., and Hu, H., "An Experimental Investigation on Rotor-to-Rotor Interactions of Small UAV Propellers," 35th AIAA Applied Aerodynamics Conference, 2017. https://doi.org/10.2514/6.2017-3744.
- [15] Alvarez, E., Schenk, A., Critchfield, T., and Ning, A., "Rotor-on-Rotor Aeroacoustic Interactions of Multirotor in Hover," *Brigham Young University Faculty Publications*, , No. 4053, 2020. URL https://scholarsarchive.byu.edu/facpub/4053.
- [16] de Vries, R., van Arnhem, N., Sinnige, T., Vos, R., and Veldhuis, L. L. M., "Aerodynamic interaction between propellers of a distributed-propulsion system in forward flight," *Aerospace Science and Technology*, Vol. 118, No. 107009, 2021. https://doi.org/10.1016/j.ast.2021.107009.
- [17] Nie, X., Shan, X., and Chen, H., A Lattice-Boltzmann / Finite-Difference Hybrid Simulation of Transonic Flow, 2009. https://doi.org/10.2514/6.2009-139.
- [18] Romani, G., Grande, E., Avallone, F., Ragni, D., and Casalino, D., "Performance and noise prediction of low-Reynolds number propellers using the Lattice-Boltzmann method," Vol. 125, No. 107086, 2022. https://doi.org/10.1016/j.ast.2021.107086.
- [19] Casalino, D., Grande, E., Romani, G., Ragni, D., and Avallone, F., "Definition of a benchmark for low Reynolds number propeller aeroacoustics," *Aerospace Science and Technology*, Vol. 113, No. 106707, 2021. https://doi.org/10.1016/j.ast.2021.106707.
- [20] Casalino, D., Avallone, F., Gonzalez-Martino, I., and Ragni, D., "Aeroacoustic study of a wavy stator leading edge in a realistic fan/OGV stage," *Journal of Sound and Vibration*, Vol. 442, 2019, pp. 138–154. https://doi.org/10.1016/j.jsv.2018.10.057.
- [21] Hanson, D., Near field noise of high tip speed propellers in forward flight, 2012. https://doi.org/10.2514/6.1976-565.
- [22] Schram, C., "Ffowcs Williams & Hawkings analogy," Lecture Notes, 2011. Von Karman Institute for Fluid Dynamics.
- [23] Roger, M., and Moreau, S., "Tonal-Noise Assessment of Quadrotor-Type UAV Using Source-Mode Expansions," Acoustics, Vol. 2, No. 3, 2020, pp. 674–690. https://doi.org/10.3390/acoustics2030036.